FERMILAB-PUB-13-102-PPD
arXiv:hep-ex/XXXX.XXXX

Measurement of Neutrino and Antineutrino Oscillations Using Beam and Atmospheric Data in MINOS

P. Adamson,[8] I. Anghel,[15,1] C. Backhouse,[21] G. Barr,[21] M. Bishai,[3] A. Blake,[5] G. J. Bock,[8] D. Bogert,[8] S. V. Cao,[29] C. M. Castromonte,[9] S. Childress,[8] J. A. B. Coelho,[30,6] L. Corwin,[14] D. Cronin-Hennessy,[18] J. K. de Jong,[21] A. V. Devan,[32] N. E. Devenish,[27] M. V. Diwan,[3] C. O. Escobar,[6] J. J. Evans,[17,16] E. Falk,[27] G. J. Feldman,[10] M. V. Frohne,[11] H. R. Gallagher,[30] R. A. Gomes,[9] M. C. Goodman,[1] P. Gouffon,[24] N. Graf,[13] R. Gran,[19] K. Grzelak,[31] A. Habig,[19] S. R. Hahn,[8] J. Hartnell,[27] R. Hatcher,[8] A. Himmel,[4] A. Holin,[16] J. Hylen,[8] G. M. Irwin,[26] Z. Isvan,[3,22] C. James,[8] D. Jensen,[8] T. Kafka,[30] S. M. S. Kasahara,[18] G. Koizumi,[8] M. Kordosky,[32] A. Kreymer,[8] K. Lang,[29] J. Ling,[3] P. J. Litchfield,[18,23] P. Lucas,[8] W. A. Mann,[30] M. L. Marshak,[18] M. Mathis,[32] N. Mayer,[30,14] A. M. McGowan,[1] M. M. Medeiros,[9] R. Mehdiyev,[29] J. R. Meier,[18] M. D. Messier,[14] D. G. Michael,[4,*] W. H. Miller,[18] S. R. Mishra,[25] S. Moed Sher,[8] C. D. Moore,[8] L. Mualem,[4] J. Musser,[14] D. Naples,[22] J. K. Nelson,[32] H. B. Newman,[4] R. J. Nichol,[16] J. A. Nowak,[18] J. O'Connor,[16] W. P. Oliver,[30] M. Orchanian,[4] R. B. Pahlka,[8] J. Paley,[1] R. B. Patterson,[4] G. Pawloski,[18,26] S. Phan-Budd,[1] R. K. Plunkett,[8] X. Qiu,[26] A. Radovic,[16] B. Rebel,[8] C. Rosenfeld,[25] H. A. Rubin,[13] M. C. Sanchez,[15,1] J. Schneps,[30] A. Schreckenberger,[18] P. Schreiner,[1] R. Sharma,[8] A. Sousa,[7,10] N. Tagg,[20] R. L. Talaga,[1] J. Thomas,[16] M. A. Thomson,[5] G. Tinti,[21] S. C. Tognini,[9] R. Toner,[10,5] D. Torretta,[8] G. Tzanakos,[2,*] J. Urheim,[14] P. Vahle,[32] B. Viren,[3] A. Weber,[21,23] R. C. Webb,[28] C. White,[13] L. Whitehead,[12,3] L. H. Whitehead,[16] S. G. Wojcicki,[26] and R. Zwaska[8]

(The MINOS Collaboration)

[1] *Argonne National Laboratory, Argonne, Illinois 60439, USA*
[2] *Department of Physics, University of Athens, GR-15771 Athens, Greece*
[3] *Brookhaven National Laboratory, Upton, New York 11973, USA*
[4] *Lauritsen Laboratory, California Institute of Technology, Pasadena, California 91125, USA*
[5] *Cavendish Laboratory, University of Cambridge, Madingley Road, Cambridge CB3 0HE, United Kingdom*
[6] *Universidade Estadual de Campinas, IFGW-UNICAMP, CP 6165, 13083-970, Campinas, SP, Brazil*
[7] *Department of Physics, University of Cincinnati, Cincinnati, Ohio 45221, USA*
[8] *Fermi National Accelerator Laboratory, Batavia, Illinois 60510, USA*
[9] *Instituto de Física, Universidade Federal de Goiás, CP 131, 74001-970, Goiânia, GO, Brazil*
[10] *Department of Physics, Harvard University, Cambridge, Massachusetts 02138, USA*
[11] *Holy Cross College, Notre Dame, Indiana 46556, USA*
[12] *Department of Physics, University of Houston, Houston, Texas 77204, USA*
[13] *Department of Physics, Illinois Institute of Technology, Chicago, Illinois 60616, USA*
[14] *Indiana University, Bloomington, Indiana 47405, USA*
[15] *Department of Physics and Astronomy, Iowa State University, Ames, Iowa 50011 USA*
[16] *Department of Physics and Astronomy, University College London, Gower Street, London WC1E 6BT, United Kingdom*
[17] *School of Physics and Astronomy, University of Manchester, Oxford Road, Manchester M13 9PL, United Kingdom*
[18] *University of Minnesota, Minneapolis, Minnesota 55455, USA*
[19] *Department of Physics, University of Minnesota Duluth, Duluth, Minnesota 55812, USA*
[20] *Otterbein College, Westerville, Ohio 43081, USA*
[21] *Subdepartment of Particle Physics, University of Oxford, Oxford OX1 3RH, United Kingdom*
[22] *Department of Physics and Astronomy, University of Pittsburgh, Pittsburgh, Pennsylvania 15260, USA*
[23] *Rutherford Appleton Laboratory, Science and Technologies Facilities Council, Didcot, OX11 0QX, United Kingdom*
[24] *Instituto de Física, Universidade de São Paulo, CP 66318, 05315-970, São Paulo, SP, Brazil*
[25] *Department of Physics and Astronomy, University of South Carolina, Columbia, South Carolina 29208, USA*
[26] *Department of Physics, Stanford University, Stanford, California 94305, USA*
[27] *Department of Physics and Astronomy, University of Sussex, Falmer, Brighton BN1 9QH, United Kingdom*
[28] *Physics Department, Texas A&M University, College Station, Texas 77843, USA*
[29] *Department of Physics, University of Texas at Austin, 1 University Station C1600, Austin, Texas 78712, USA*
[30] *Physics Department, Tufts University, Medford, Massachusetts 02155, USA*
[31] *Department of Physics, University of Warsaw, Hoża 69, PL-00-681 Warsaw, Poland*
[32] *Department of Physics, College of William & Mary, Williamsburg, Virginia 23187, USA*

(Dated: April 23, 2013)

We report measurements of oscillation parameters from ν_μ and $\overline{\nu}_\mu$ disappearance using beam and atmospheric data from MINOS. The data comprise exposures of 10.71×10^{20} protons on target (POT) in the ν_μ-dominated beam, 3.36×10^{20} POT in the $\overline{\nu}_\mu$-enhanced beam, and 37.88 kton-years of atmospheric neutrinos. Assuming identical ν and $\overline{\nu}$ oscillation parameters, we measure $|\Delta m^2| = (2.41^{+0.09}_{-0.10}) \times 10^{-3}\,\mathrm{eV}^2$ and $\sin^2(2\theta) = 0.950^{+0.035}_{-0.036}$. Allowing independent ν

Operated by Fermi Research Alliance, LLC under Contract No. De-AC02-07CH11359 with the United States Department of Energy.

and $\overline{\nu}$ oscillations, we measure antineutrino parameters of $|\Delta\overline{m}^2| = (2.50^{+0.23}_{-0.25}) \times 10^{-3}\,\mathrm{eV}^2$ and $\sin^2(2\overline{\theta}) = 0.97^{+0.03}_{-0.08}$, with minimal change to the neutrino parameters.

PACS numbers: 14.60.Pq, 14.60.Lm, 29.27.-a

Neutrino oscillation provides direct evidence that neutrinos have non-zero mass and represents the only phenomenon observed to date with an origin beyond the Standard Model of particle interactions. With massive neutrinos, three flavor eigenstates mix with three mass eigenstates according to a unitary matrix that can be parameterized by three angles and a CP-violating phase [1]. The resulting oscillation probability depends on the mixing angles and on the differences between the squared neutrino masses. The MINOS experiment performs precision measurements of oscillations via ν_μ disappearance. These oscillations are well described by an effective two-flavor model with flavor and mass eigenstates related by a single mixing angle θ. In this approximation, the ν_μ survival probability is given by

$$P(\nu_\mu \to \nu_\mu) = 1 - \sin^2 2\theta \, \sin^2\left(\frac{1.267\ \Delta m^2[\mathrm{eV}^2]\ L[\mathrm{km}]}{E[\mathrm{GeV}]}\right),$$

where L is the distance traveled by the neutrino and E is its energy. The mass splitting, Δm^2, is an admixture of the three-flavor parameters Δm^2_{31} and Δm^2_{32} [2], and it differs from Δm^2_{32} by less than 2%. The $\overline{\nu}_\mu$ survival probability has the same form, but the mixing parameters are denoted by $\Delta\overline{m}^2$ and $\sin^2(2\overline{\theta})$.

The MINOS measurements use neutrinos produced in the NuMI accelerator complex and by cosmic ray interactions in the atmosphere. The accelerator provides a source of neutrinos with a fixed baseline and an energy spectrum that peaks at $L/E \sim 250\,\mathrm{km/GeV}$, close to the region where the ν_μ survival probability reaches its first minimum. Atmospheric neutrinos are produced with a broad range of $E(\sim 0.5 - 10^4\,\mathrm{GeV})$ and $L(\sim 10 - 10^4\,\mathrm{km})$, enabling the study of oscillations across a wide region in L/E and covering many oscillation cycles. The precision of the oscillation measurement is enhanced by combining these two complementary samples.

This Letter presents the first ever joint analysis of atmospheric and accelerator neutrinos in the same experiment. The new results come from the full MINOS data set, collected over a period of nine years. The combination of data sets, together with increased exposures, produces a significant improvement in the sensitivity to oscillations over previous MINOS analyses [3–6]. Furthermore, MINOS has the unique ability to separate neutrinos and antineutrinos on an event-by-event basis. Coupled with the world's only set of long-baseline accelerator antineutrino data, we present the most precise measurements to date of the larger mass splitting for both neutrinos and antineutrinos.

The NuMI beam [7] is produced at the Fermi National Accelerator Laboratory (Fermilab) by 120 GeV protons striking a graphite target. The resulting charged pions and kaons are focused by two magnetic horns before decaying in a 675 m long helium-filled volume [8]. The beam is directed through a hadron absorber and rock to stop all particles except neutrinos. The energy spectrum of the neutrino beam can be changed by varying the distance between the target and first horn. Most of the data used in this analysis were collected with a spectrum peaking at a neutrino energy of 3 GeV. By selectively focusing positive or negative pions and kaons, a ν_μ-dominated or $\overline{\nu}_\mu$-enhanced beam is produced.

The two MINOS detectors are steel-scintillator tracking calorimeters with toroidal magnetic fields [9]. Each detector consists of steel plates with segmented plastic scintillator planes mounted on them. The planes are perpendicular to the beam direction. The 0.98 kton Near Detector (ND), located 1.04 km from the neutrino production target, measures the beam composition and energy near the source. The 5.4 kton Far Detector (FD) measures the beam composition and energy spectrum 735 km away from the target. Installed 705 m (2070 m water-equivalent) underground in the Soudan Underground Laboratory in Minnesota, the FD is also used to measure oscillations in atmospheric neutrinos and antineutrinos. A scintillator veto shield is installed above the FD to enhance the rejection of the cosmic-ray muon background.

Muon neutrinos and antineutrinos are identified through their charged current (CC) interactions

$$\nu_\mu(\overline{\nu}_\mu) + X \to \mu^-(\mu^+) + X'.$$

The muon typically deposits energy in the detector in a clear track-like pattern. The hadronic recoil system, X', leaves a diffuse shower-like deposition pattern. The only notable background in the CC sample arises from a small number of neutral current (NC) interactions that generate only hadronic activity but can display a track-like signature. Muon neutrinos and antineutrinos are separated by the direction of curvature of the charged muon track in the magnetic field of the detectors. The muon momentum is determined from the range for muons that stop in the detector and from curvature for exiting muons. For beam neutrino interactions, a k-Nearest-Neighbor classification algorithm (kNN) is used to estimate the hadronic energy from both the calorimetric energy deposited and the topology of the shower [10]. For atmospheric neutrino interactions, the calorimetric energy deposits in each scintillator strip are summed to provide an estimate of the true shower energy. The reconstructed neutrino energy is given by the sum of the muon and shower energy measurements.

Our new results are based on FD exposures of 10.71×10^{20} protons on target (POT) in the ν_μ-dominated beam and 3.36×10^{20} POT in the $\overline{\nu}_\mu$-enhanced beam, corresponding to increases of 48% and 14%, respectively, over our previous analyses [3, 5]. As in these previous analyses, the selection of ν_μ and $\overline{\nu}_\mu$ CC interaction candidates proceeds via the construction of a set of variables that characterize the event topology and energy deposition of muon tracks [11]. Again, these variables are combined into a single discriminating variable using a kNN technique.

From the ν_μ-dominated beam, we use both neutrinos and antineutrinos with interaction vertices contained within the detectors' fiducial volumes. When explicitly fitting antineutrino oscillation parameters, we apply an optimized antineutrino event selection to increase the purity of this contained-vertex antineutrino sample [6]. In this beam mode, we also select a sample of non-fiducial muons in the FD, comprising ν_μ CC and $\overline{\nu}_\mu$ CC interactions outside the fiducial volume and in the rock surrounding the detector [12, 13]. No muon charge-sign separation is performed on this sample since many of these muons are confined to the edges of the detector where the magnetic field is very low and muon curvature is less well modeled. In the $\overline{\nu}_\mu$-enhanced beam, only the contained-vertex antineutrino sample is used, as the non-fiducial sample is dominated by high energy neutrinos.

The predicted FD beam spectra are derived from the observed ND beam data using a beam transfer matrix [14]. This extrapolation procedure mitigates many sources of systematic uncertainties and naturally accounts for any variations in the beam conditions such as target degradation or differences among the seven different production targets used throughout the experiment's lifetime. Since the ND is used to provide a baseline spectrum, it is important to minimize any differences between the response in the two detectors. In particular, the region around the ND magnetic coil is poorly modeled, so any beam-induced events with muon tracks entering this region are removed from the ND data set.

We use the same atmospheric neutrino data set and event samples as our previous analysis [4], which is based on a FD exposure of 37.88 kton-years. The events are identified by the presence of either an interaction vertex within the fiducial volume of the detector or an upward-going or horizontal muon track. The selected events are separated into three samples: contained-vertex muons, non-fiducial muons, and contained-vertex showers. The two muon samples are produced by ν_μ CC and $\overline{\nu}_\mu$ CC interactions; the contained-vertex shower sample is composed mainly of ν_e CC, $\overline{\nu}_e$ CC and NC interactions. The atmospheric neutrino samples must be selected from a background of cosmic-ray muons. For contained-vertex muons and showers, this background is reduced to 4% and 12%, respectively, by applying a series of containment requirements and by checking for energy deposits in the sections of veto shield above the fiducial event vertex within a ± 50 ns window. In the non-fiducial sample, the background is almost entirely removed by using the 2.5 ns timing resolution to accurately determine the incoming muon track direction. Table I lists the numbers of observed events and the corresponding predictions, with and without oscillations, for each of the analyzed samples.

Data Set	Simulation No osc.	Simulation With osc.	Events Observed
ν_μ from ν_μ beam	3201	2543	2579
$\overline{\nu}_\mu$ from ν_μ beam	363	324	312
Non-fiducial μ from ν_μ beam	3197	2862	2911
$\overline{\nu}_\mu$ from $\overline{\nu}_\mu$ beam	313	227	226
Atm. contained-vertex $\nu_\mu + \overline{\nu}_\mu$	1100	881	905
Atm. non-fiducial $\mu^- + \mu^+$	570	467	466
Atm. showers	727	724	701

TABLE I: Numbers of events selected in each sample. The oscillated event yields come from the best fit to all data, assuming identical ν and $\overline{\nu}$ oscillations.

We simulate atmospheric neutrino events according to the Bartol flux calculations [15]. The beam neutrino flux is simulated using the FLUGG [16] package, which combines GEANT4 [17] geometry with FLUKA [16] hadron production. All beam neutrino interactions, and interactions of atmospheric neutrinos in the detectors, are simulated using NEUGEN3 [18]. We simulate atmospheric neutrino interactions in the surrounding rock using NUANCE [19], which propagates the final-state muons through the rock and up to the edge of the detector. In both the beam and atmospheric simulations, the propagation of particles in the detector, and the detector response, are simulated with GCALOR [20] and GEANT3 [21]. The simulation incorporates the background arising from $\nu_\mu \to \nu_\tau$ appearance. For the best fit oscillations, the predicted event yield from this channel totals 18 events across the entire data set.

The oscillation parameters are obtained from a maximum likelihood fit to the data. The measured FD beam data are binned as a function of reconstructed neutrino energy. To improve the sensitivity of the analysis, the contained-vertex ν_μ events from the ν_μ-dominated beam are divided into five sub-samples according to their estimated energy resolution, which lies primarily in the range $5 - 30\%$ [22, 23]. The atmospheric samples are binned as a function of L/E. The contained-vertex atmospheric ν_μ and $\overline{\nu}_\mu$ events are divided into four sub-samples according to the estimated $L[\mathrm{km}]/E[\mathrm{GeV}]$ resolution, where $\sigma_{\log_{10}(L/E)}$ ranges from 0.05 to 1.2 [24]. The contained-vertex showers are grouped in a single bin because the majority are too short for an accurate measurement of L/E. These events are relatively insensitive to oscillations but provide a constraint on the overall normalization of the atmospheric flux.

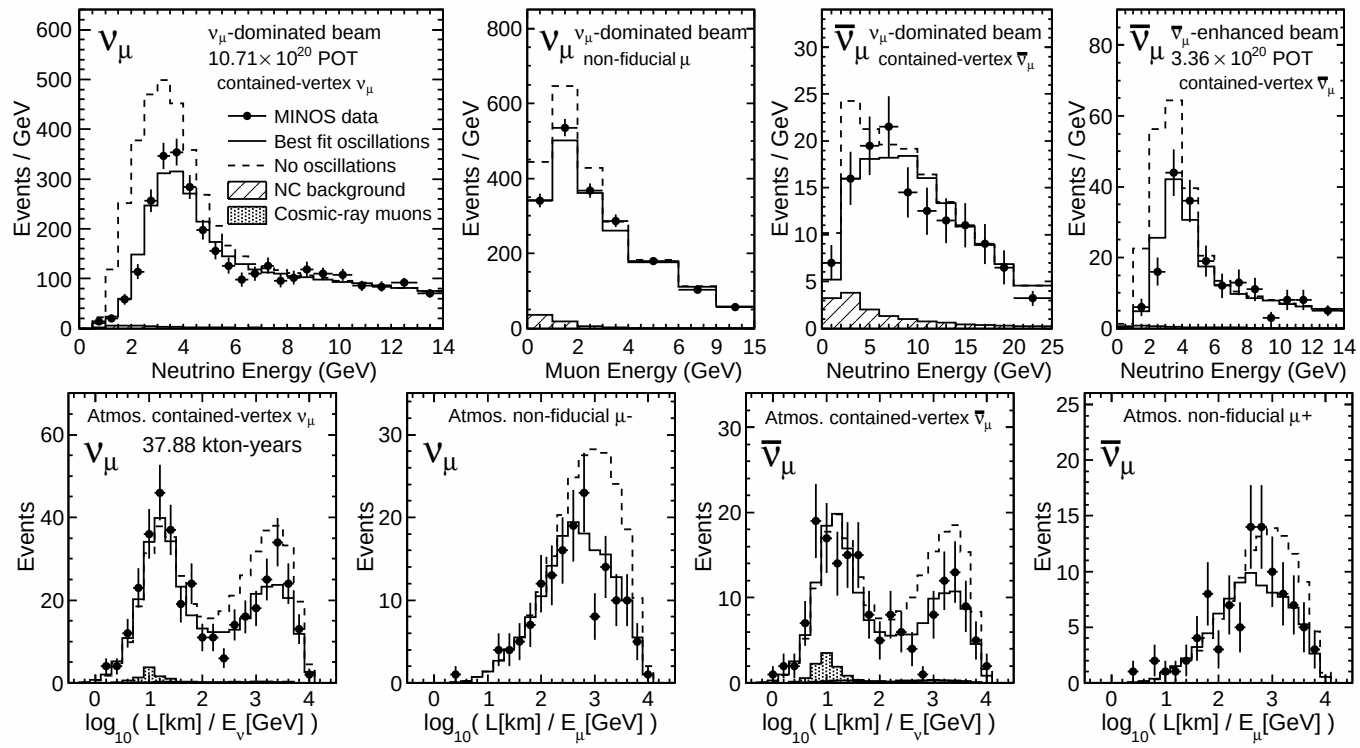

FIG. 1: FD data samples compared to predictions with and without oscillations. The top row shows the energy spectra of the beam samples, while the bottom row shows the L/E distributions for the atmospheric event samples.

The fit incorporates a set of nuisance parameters that accommodate the largest systematic uncertainties in the simulation of the beam [3, 5] and the atmospheric [4] neutrino data. For both data sets, the fit incorporates the systematic uncertainties in the overall normalizations of the event samples, the relative normalization of the NC background component, the muon momentum, and the shower energy. The latter two uncertainties are taken as correlated between the beam and atmospheric samples. An analysis performed with all uncertainties uncorrelated produces similar results. Additional systematic parameters are included in the fit to cover the uncertainties in the rate and spectral shape of atmospheric ν_μ and $\overline{\nu}_\mu$ events arising from uncertainties in the neutrino flux and cross-section simulations.

When we fit the full MINOS data sample to the two-flavor neutrino oscillation hypothesis, assuming that neutrinos and antineutrinos have identical oscillation parameters, we obtain $|\Delta m^2| = (2.41^{+0.09}_{-0.10}) \times 10^{-3}\,\mathrm{eV}^2$ and $\sin^2(2\theta) = 0.950^{+0.035}_{-0.036}$. Maximal mixing is disfavored at the 86% confidence level (C.L.); we measure $\sin^2(2\theta) > 0.890$ at 90% C.L. The observed beam and atmospheric event spectra in the FD are shown in Fig. 1, along with the predictions for the case of no oscillations and the best fit. The data are well described by the neutrino oscillation model; the same analysis performed on simulated experiments returns a worse quality of fit for 19.1% of those experiments. A number of cross checks were performed by fitting each of the data samples separately. Those separate fits yielded consistent oscillation parameters, indicating that the data samples are consistent with each other and with the oscillation hypothesis. Allowed regions for the oscillation parameters, assuming identical neutrino and antineutrino oscillations, are shown in Fig. 2.

The magnetized MINOS detectors enable separation of neutrino and antineutrino interactions for both beam and atmospheric events, allowing an independent measurement of the antineutrino oscillation parameters. We perform an additional fit in which we allow neutrinos and antineutrinos to have different oscillation parameters, and find $|\Delta\overline{m}^2| = (2.50^{+0.23}_{-0.25}) \times 10^{-3}\,\mathrm{eV}^2$ and $\sin^2(2\overline{\theta}) = 0.97^{+0.03}_{-0.08}$ (> 0.83 at 90% C.L.). The difference between the antineutrino and neutrino mass splittings is measured to be $|\Delta\overline{m}^2| - |\Delta m^2| = (0.12^{+0.24}_{-0.26}) \times 10^{-3}\,\mathrm{eV}^2$. Corresponding measurements using the beam and atmospheric samples separately yield consistent results. The 90% C.L. allowed region for the antineutrino oscillation parameters is shown in Fig. 3, illustrating good agreement between the measured neutrino and antineutrino oscillation parameters.

In summary, we have presented an analysis of the combined MINOS beam and atmospheric neutrino sam-

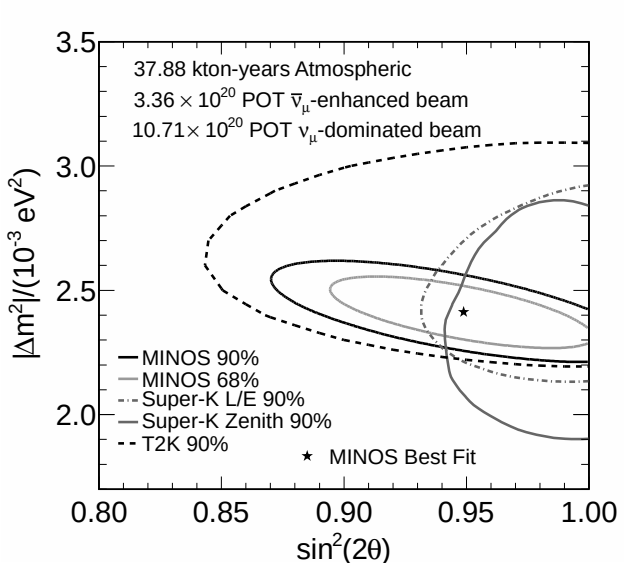

FIG. 2: The allowed regions of $|\Delta m^2|$ and $\sin^2(2\theta)$, assuming identical neutrino and antineutrino oscillations. The MINOS result is compared to results from Super-Kamiokande [25] and T2K [26].

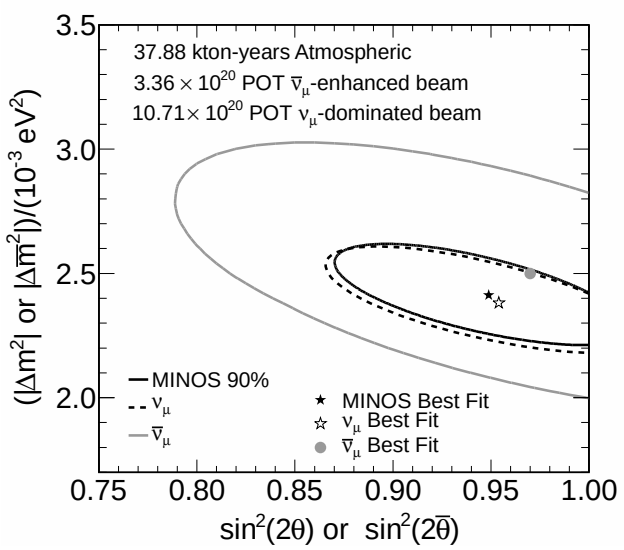

FIG. 3: The 90% confidence level allowed region of $|\Delta m^2|$ and $\sin^2(2\theta)$ from the fit assuming identical neutrino and antineutrino oscillations (MINOS 90%, also in Fig. 2) is compared to the allowed regions for ν_μ and $\overline{\nu}_\mu$ from the fit in which neutrinos and antineutrinos have different oscillation parameters.

ples, representing the complete data set from the MINOS experiment. Assuming that neutrinos and antineutrinos share identical oscillation parameters, we measure $\sin^2(2\theta) = 0.950^{+0.035}_{-0.036}$ (> 0.890 at 90% C.L.) and $|\Delta m^2| = (2.41^{+0.09}_{-0.10}) \times 10^{-3}\,\mathrm{eV}^2$. Allowing independent oscillations, we measure antineutrino parameters of $\sin^2\left(2\overline{\theta}\right) = 0.97^{+0.03}_{-0.08}$ (> 0.83 at 90% C.L.) and $|\Delta\overline{m}^2| = (2.50^{+0.23}_{-0.25}) \times 10^{-3}\,\mathrm{eV}^2$. A comparison of the neutrino and antineutrino mass splittings shows them to be in excellent agreement. These results provide the world's most precise measurement to date of these mass splittings for both neutrinos and antineutrinos.

This work was supported by the U.S. DOE; the United Kingdom STFC; the U.S. NSF; the State and University of Minnesota; the University of Athens, Greece; Brazil's FAPESP, CNPq and CAPES. We are grateful to the Minnesota Department of Natural Resources and the personnel of the Soudan Laboratory and Fermilab. We thank Texas Advanced Computing Center at The University of Texas at Austin for the provision of computing resources.

---

* Deceased.
[1] J. Beringer *et al.* (Particle Data Group), Phys. Rev. D **86**, 010001 (2012).
[2] G. L. Fogli *et al.*, Prog. Part. Nucl. Phys. **57**, 742 (2006); H. Nunokawa *et al.*, Phys. Rev. D **72**, 013009 (2005).
[3] P. Adamson *et al.* (MINOS), Phys. Rev. Lett. **106**, 181801 (2011).
[4] P. Adamson *et al.* (MINOS), Phys. Rev. D **86**, 052007 (2012).
[5] P. Adamson *et al.* (MINOS), Phys. Rev. Lett. **108**, 191801 (2012).
[6] P. Adamson *et al.* (MINOS), Phys. Rev. D **84**, 071103 (2011).
[7] K. Anderson *et al.*, FERMILAB-DESIGN-1998-01 (1998).
[8] For the first 3.36×10^{20} POT of data taking with the ν_μ-dominated beam, the decay pipe was evacuated; it was then filled with helium at a pressure of 0.9 atm for structural reasons.
[9] D. G. Michael *et al.* (MINOS), Nucl. Instrum. Meth. A **596**, 190 (2008).
[10] C. Backhouse, D.Phil. thesis, U. of Oxford (2011).
[11] R. Ospanov, Ph.D. thesis, U. of Texas at Austin (2008).
[12] M. L. Strait, Ph.D. thesis, U. of Minnesota (2010).
[13] A. McGowan, Ph.D. thesis, U. of Minnesota (2007).
[14] P. Adamson *et al.* (MINOS), Phys. Rev. D **77**, 072002 (2008).
[15] G. D. Barr *et al.*, Phys. Rev. D **70**, 023006 (2004).
[16] G. Battistoni *et al.*, AIP Conf. Proc. **896**, 31 (2007).
[17] K. Amako *et al.* (GEANT4), IEEE Trans. on Nucl. Sci. **53**, 270 (2006).
[18] H. Gallagher, Nucl. Phys. Proc. Suppl. **112**, 188 (2002).
[19] D. Casper, Nucl. Phys. Proc. Suppl. **112**, 161 (2002).
[20] C. Zeitnitz and T. A. Gabriel, Nucl. Instrum. Meth. A **349**, 106 (1994).
[21] Application Software Group, CERN Program Library Long Writeup W5013 (CERN, 1994).
[22] S. J. Coleman, Ph.D. thesis, Coll. of William & Mary (2011).
[23] J. Mitchell, Ph.D. thesis, U. of Cambridge (2011).
[24] A. Blake *et al.*, Nucl. Instrum. Meth. A **707**, 127 (2013).
[25] Y. Itow, in *Proceedings of the 25th International Conference on Neutrino Physics and Astrophysics (Neutrino 2012), Kyoto, Japan, June 2012*, to be published.
[26] K. Abe *et al.* (T2K), Phys. Rev. D **85**, 031103 (2012).